THE JOURNAL OF BIOLOGICAL CHEMISTRY VOL. 288, NO. 49, pp. 35437–35451, December 6, 2013

Interactome Analysis Reveals Ezrin Can Adopt Multiple Conformational States*[S]

Received for publication, July 30, 2013, and in revised form, October 18, 2013 Published, JBC Papers in Press, October 22, 2013, DOI 10.1074/jbc.M113.505669

Raghuvir Viswanatha[1], **Jessica Wayt**[1], **Patrice Y. Ohouo**[1], **Marcus B. Smolka, and Anthony Bretscher**[2]

From the Department of Molecular Biology and Genetics and Weill Institute for Cell and Molecular Biology, Cornell University, Ithaca, New York 14853

Background: Ezrin is a conformationally regulated microfilament-membrane linker restricted to the apical aspect of epithelial cells.
Results: Quantitative mass spectrometry identified proteins that associate with different ezrin conformations; the interactors include novel apical microvilli-associated proteins, with classes perceiving ezrin's conformation differentially.
Conclusion: Different proteins selectively associate with three distinct conformational states of ezrin.
Significance: This study extends the conformational activation model of ezrin and identifies new interacting partners.

Ezrin, a member of the ezrin-radixin-moesin family (ERM), is an essential regulator of the structure of microvilli on the apical aspect of epithelial cells. Ezrin provides a linkage between membrane-associated proteins and F-actin, oscillating between active/open and inactive/closed states, and is regulated in part by phosphorylation of a C-terminal threonine. In the open state, ezrin can bind a number of ligands, but in the closed state the ligand-binding sites are inaccessible. *In vitro* analysis has proposed that there may be a third hyperactivated form of ezrin. To gain a better understanding of ezrin, we conducted an unbiased proteomic analysis of ezrin-binding proteins in an epithelial cell line, Jeg-3. We refined our list of interactors by comparing the interactomes using quantitative mass spectrometry between wild-type ezrin, closed ezrin, open ezrin, and hyperactivated ezrin. The analysis reveals several novel interactors confirmed by their localization to microvilli, as well as a significant class of proteins that bind closed ezrin. Taken together, the data indicate that ezrin can exist in three different conformational states, and different ligands "perceive" ezrin conformational states differently.

The establishment and maintenance of cell polarity are carried out through the asymmetrical distribution of macromolecules. An important contributor to the structure of microvilli on the apical aspect of epithelial cells is the F-actin-binding protein ezrin. Ezrin, the founding member of the conserved ezrin-radixin-moesin (ERM) protein family, was originally isolated from the intestinal brush border (1) and later shown to play essential roles in cell polarity throughout animal development (2). Ezrin adopts a highly polarized distribution in epithelial cells where it is found both in the cytoplasm and specifically associated with the microvillar plasma membrane. Consistently, it is essential for the normal morphology of microvilli *in vivo* (3–6) and in cultured cells (6, 7).

In their inactive state, ERMs undergo an intramolecular head-to-tail association, masking binding sites for both plasma membrane-associated proteins on their N-terminal four-point-one ezrin-radixin-moesin (FERM) domain and the F-actin-binding site in the C-terminal tail. The appearance of ezrin in its active state on the microvillar plasma membrane requires direct interaction with the membrane phospholipid $PI(4,5)P_2$ through its N-terminal FERM domain (8–12) followed by phosphorylation on a conserved C-terminal threonine (Thr-567 in ezrin (7, 8, 13)). In epithelial cells, kinase and phosphatase activity drives constant, dynamic interconversion between membrane-bound phosphorylated ezrin and cytoplasmic dormant, unphosphorylated ezrin, with each state having a half-life of 1–2 min (7, 14, 15).

Although ezrin is generally considered to simply oscillate between open/active or closed/inactive states, there are likely to be varying degrees of ezrin openness, reflecting the existence of multiple conformational states. Notably, *in vitro* analysis has suggested that phosphorylation of the C-terminal threonine in ezrin creates a partial but not fully open state (16). Thus, we explored this possibility by examining two forms of open ezrin in our analysis.

Upon reaching the plasma membrane, ERM proteins engage a number of membrane-associated factors through the N-terminal FERM domain. Numerous binding partners of mammalian ERMs have been identified (Table 1). In most of these interactions, the interacting protein has been proposed to be the effector as opposed to being the regulator of ERMs. Conversely, one of these, the scaffolding ERM-binding phosphoprotein 50 (EBP50, also known as NHERF1 or SLC9A3R1), has been shown to regulate the ERM-dependent formation of microvilli (17–19). However, transmembrane ERM-binding proteins have also been proposed to play a role in ERM recruitment or clustering in the apical domain leading to the formation of microvilli (20), although no such protein has yet been identified in epithelial cells. Moreover, *in vitro* analyses show that although the surfaces on the FERM domain for EBP50, $PI(4,5)P_2$, and transmembrane proteins are distinct (10,

* This work was supported, in whole or in part, by National Institutes of Health Grant GM-036652 (to A. B.).
[S] This article contains supplemental Table S1.
[1] Supported in part by National Institutes of Health Training Grant 5T32GM007273.
[2] To whom correspondence should be addressed: Weill Institute for Cell and Molecular Biology, 257 Weill Hall, Cornell University, Ithaca, NY 14853. Tel.: 607-255-5709; E-mail: apb5@cornell.edu.

21–25), there is likely to be a complex interplay among all of these ligands (26). Thus, multiple regulatory ERM binding partners might be identified by an unbiased proteomic screen for ERM-binding proteins in epithelial cells.

Here, we report the first global analysis of ezrin binding partners in an epithelial cell line. We first established a reversible cross-linking strategy that preserves the transient interaction between ezrin and its strongest known interactor, EBP50. We then used mass spectrometry to determine the ezrin interactome under these optimized conditions. Next, we examined how the ezrin interactome changes depending on its conformational state, and we documented the changes in response to ezrin conformation. The analysis reveals many novel components of microvilli that discriminate between different open forms, as well as an unexpected category of proteins binding to the closed form of ezrin.

EXPERIMENTAL PROCEDURES

Plasmids—Plasmids for stable or transient transfection of ezrin-iFLAG and variants (in pQCXIP, Clontech) have been previously described (7). The "K4N" mutation (22) was generated by inverse PCR (using primers 5′-CCC ATC GAC AAC AAC GCA CCT GAC TTT GTG TTT TAT GCC CCA C-3′ and 5′-TTT AAT GAC AAA GTT ATT GTC ATT GAA AGA GAT GTT CCT GAT TTC ACT CC-3′). To clone TACTSTD2, BASP1, SLC1A5, FAM129B, and EPCAM, Jeg-3 RNA was first extracted using the RNeasy kit (Qiagen) and then reverse-transcribed using the SuperScript III reverse transcriptase poly(dT) primer (Invitrogen). The open reading frames were cloned from the cDNA using PCR (with the following primers: TACSTD2, 5′-GTT CGA GGA TCC ATG GCT CGG GGC CCC GGC-3′ and 5′-TCG AAC GAA TTC CAA GCT CGG TTC CTT TCT CAA CTC CC-3′; BASP1, 5′-GTT CGA GGA TCC ACC ATG GGA GGC AAG CTC AGC AAG AAG AAG-3′ and 5′-TCG AAC GAA TTC CTC TTT CAC GGT TAC GGT TTG GTC GG-3′; SLC1A5, 5′-GTT CGA GAA TTC ACC ATG GTG GCC GAT CCT CCT CGA GAC-3′ and 5′-TCG AAC GCG GCC GCt tCA TGA CTG ATT CCT TCT CAG AGG CGA CC-3′) and then inserted into pEGFP-N2 (Clontech) and pcDNA3.1/MycHisA (Invitrogen). GFP-FHOD1 was generated by PCR from an ATCC cDNA clone and insertion into pEGFP-C2. GFP-CLIC4 expression plasmid was a gift of Dr. M. Berryman, Ohio University, Athens, OH. SCYL3-myc expression plasmid was a gift of Dr. R. Thorne, University of Newcastle, Australia. The following constructs were examined and reported in Fig. 5*H* without images: FAM129B, cloned from Jeg-3 cDNA by PCR (using primers 5′-GGG GAC AAG TTT GTA CAA AAA AGC AGG CTT TAT GGG GGA CGT GCT GTC CAC GC-3′ and 5′-GGG GAC CAC TTT GTA CAA GAA AGC TGG GTA GAA CTC AGT CTG CAC CCC TGC ACT G-3′), inserted into pDONR221 (Invitrogen), and then recombined into pcDNA-DEST47 (Invitrogen); EPCAM, cloned from Jeg-3 cDNA by PCR (using primers 5′-GTT CGA CTC GAG ATG GCG CCC CCG CAG GTC C-3′ and 5′-TCG AAC GAA TTC TGC ATT GAG TTC CCT ATG CAT CTC ACC C-3′) and inserted into pcDNA3.1/V5HisA; ATP11C-HA, a gift of Dr. H. W. Shin, University of Kyoto, Japan, which was co-expressed with Cdc50A as described (27); LOK and SLK, reported previously (7); F11R (also known as junction adhesion molecule A) with an internal HA tag, a gift of Dr. U. Naik, University of Delaware; ARHGAP18, ID HsCD00379004, from the Dana-Farber/Harvard Cancer Center recombined into pcDNA-DEST47.

Antibodies—FLAG antibody and resin were M2 from Sigma. Antibody against ezrin was CPCT-Ezrin-1; moesin was CPCT-Moesin-1, and β-dystroglycan (DAG1) was MANDAG2, all from the Developmental Studies Hybridoma Bank. Antibody against an epitope present in all ERMs was from Cell Signaling Technologies. Antibodies against radixin and EBP50 have been described (7, 28). Antibody against FHOD-1 was from Abcam. Antibody against Myc was 9E10 from Roche Applied Science. Antibody against GFP was from Santa Cruz Biotechnology. Antibody against HA was HA.11 from Covance. Antibody against TACSTD2 was GA733.1 (immunofluorescence) from Abcam or H-85 from Santa Cruz Biotechnology (Western blot).

Cell Culture, Transfection, and Stable Cell Line Creation—Jeg-3 cells were obtained from the American Type Culture Collection and cultured in minimal Eagle's medium supplemented with GlutaMAX-1 (Invitrogen), penicillin/streptomycin (Invitrogen), and 10% FBS (Invitrogen) and maintained at 37 °C and 5% CO_2.

All transient transfections were by polyethyleneimine (PolyPlus) as described previously (17). Following transfection, cells were grown for ~18 h prior to use.

Stable cell lines expressing ezrin-iFLAG variants were transfected as described previously (7) and then batch-selected using puromycin (2 μg/ml). Stable cell lines expressing BASP-1-GFP and SLC1A5-GFP were generated by transfection with the appropriate plasmid, grown in G418 (400 μg/ml) for 2 weeks, and ring-cloned and pooled at least three GFP-expressing colonies.

SILAC[3] *Labeling*—Jeg-3 cells stably transfected with pQCXIP and derivatives and then selected for at least 2 weeks were grown for at least 2 additional weeks in SILAC minimal Eagle's medium (Thermo) containing 0.1 mg/ml normal lysine and arginine ("light") or [$^{13}C_6$,$^{15}N_2$]lysine and [$^{13}C_6$,$^{15}N_4$]arginine ("heavy," Sigma) containing 10% dialyzed FBS (Invitrogen), penicillin/streptomycin (Invitrogen), and puromycin (2 μg/ml). Incorporation was verified by mixing lysate preparations from heavy and light cells (1:1) followed by mass spectrometry. Expected morphology and ezrin-iFLAG localization after labeling was verified by immunofluorescence (data not shown).

Dithiobis(succinimidyl Propionate) (DSP) Cross-linking—Cells grown to ~80% confluence were washed three times with PBS and treated with 1.25 mM DSP (Thermo) at 37 °C for 2 min. The cells were then removed to room temperature and washed three times with TBS. They were incubated in the last TBS wash for 15–20 min prior to use. Expected morphology and ezrin-iFLAG localization after labeling were verified by immunofluorescence (data not shown).

[3] The abbreviations used are: SILAC, stable isotope labeling in cell culture; MLS, microvilli-like structure; DSP, dithiobis(succinimidyl propionate); $PI(4,5)P_2$, phosphatidylinositol 4,5-biphosphate.

Immunoprecipitation and Mass Spectrometry—For SILAC mass spectrometry, ~4×10^7 DSP-treated heavy and the same number of light cells were independently scraped into cold IP buffer (25 mM Tris, pH 7.4, 5% glycerol, 150 mM NaCl, 50 mM NaF, 0.1 mM sodium orthovanadate, 10 mM β-glycerophosphate, 8.7 mg/ml *para*-nitrophenyl phosphate, 0.5% Triton X-100, 0.1 μM calyculin A, protease inhibitor table from Roche Applied Science), incubated for 2–3 h in the cold using 20 μl of FLAG M2 affinity gel (Sigma), and then washed four times in IP wash buffer (25 mM Tris, pH 7.4, 5% glycerol, 150 mM NaCl, 50 mM NaF, 0.2% Triton X-100). Gel was then eluted by boiling in 50 mM Tris, pH 8.0, containing 1% SDS, reduced, and alkylated. Proteins were precipitated with 50:49.9:0.1, acetone/ethanol/acetic acid, reconstituted in urea solution, and trypsin-digested overnight. Peptides were then purified on a C-18 column (Waters), dried, and reconstituted in 80% acetonitrile and 1% formic acid and fractionated by hydrophilic interaction chromatography. Fractions were dried, reconstituted in 0.1% trifluoroacetic acid, and analyzed by LC-MS/MS using an Orbitrap XL mass spectrometer (Thermo). Database search and peptide quantification of heavy/light isotope ratios were performed as described previously (29). Criteria for selection of true interactors are presented under "Results."

For all other immunoprecipitations, ~8×10^6 cells transfected with 7 μg of appropriate plasmid(s) were lysed in IP buffer, immunoprecipitated with 4 μl of FLAG M2 affinity gel for 2–3 h, washed four times with IP wash buffer, eluted by addition of 3×FLAG peptide to 200 μg/ml, and incubated for 10 min at room temperature. Soluble material was separated in a spin column (Sigma), denatured by boiling in Laemmli buffer, and resolved by SDS-PAGE.

Immunofluorescence—Cells grown on glass coverslips were fixed in 3.7% formaldehyde/PBS for 15 min at room temperature. Cells were then washed with PBS and blocked with IF buffer (PBS + 0.5% BSA + 0.5% goat serum + 0.1% Triton X-100) for 10 min. Primary and secondary antibodies were then applied in IF buffer with 1% FBS. After antibody addition, the coverslips were washed three times in PBS, mounted in Vectashield (Vector Laboratories), imaged using a CSU-X spinning disk microscope (Intelligent Imaging Innovations) with a spherical aberration correction device, 63 × 1.4 NA objective on an inverted microscope (Leica), and acquired with a QuantEM EMCCD camera using Slidebook software (Intelligent Imaging Innovations). Maximum intensity projections were assembled in Slidebook and exported to Adobe Illustrator software. For clarity, side projections were vertically expanded 3-fold using Illustrator.

RNA Interference—Jeg-3 cells were transfected with 30 nM of siRNA for 72 h prior to use by using Lipofectamine RNAiMAX (Invitrogen) according to the manufacturer's instructions. siRNAs were from Ambion, Dharmacon, or Integrated DNA Technologies as follows: GL2 luciferase (17), ezrin (7), radixin (5′-UGAAGAUGUUUCUGAGGAAdUdU-3′), TACSTD2 (−1, 5′-GCUUAAAUGAGUUUAGAUGGGAAAT-3′ and −2, 5′-GCUUAAAUGAGUUUAGAUGGGAAAT-3′), and DAG1 (5′-CCCUAGAGCCUGACUUUAAdTdT-3′).

RESULTS

Cross-linking Prior to Immunoprecipitation Is Required to Recover the Ezrin-EBP50 Interaction—Since its discovery in 1983 (1), numerous proteins have been shown to interact with ezrin (Table 1). Among the most tenacious *in vitro* interaction partner is EBP50 (SLC9A3R1), a scaffolding protein that binds with very high affinity through its C-terminal region to the FERM domain of ezrin (28). The binding site for EBP50 on the FERM domain is masked in the closed, inactive form of ezrin (21, 28, 30). Our goal was to perform an unbiased screen for proteins present in epithelial cells that bind to active ezrin *in vivo*, and EBP50 was used as a positive control to establish optimal conditions.

Our strategy centers around the generation of cell lines expressing various mutants of ezrin representing various conformational states and then analyzing the bound proteins that are co-recovered with ezrin. As reported recently, we have placed a FLAG epitope into an internal region of ezrin that is poorly conserved in ERM proteins (7). Using this tagged version designated ezrin-iFLAG, we have generated stable Jeg-3 choriocarcinoma cell lines that express wild-type ezrin (ezrin-iFLAG), a variant with the activating T567E phosphomimetic mutation (ezrin-T567E-iFLAG), an inactive variant with the nonphosphorylatable T567A mutation (ezrin-T567A-iFLAG), and a variant containing a truncation of the C terminus that compromises the normal FERM/C-terminal tail interaction to expose the fully unmasked FERM domain of ezrin (ezrin(1–583)-iFLAG). The level of the ezrin-iFLAG variant expression in these cells is about the same as endogenous ezrin (7). As expected, ezrin-iFLAG localization was strictly apical, co-localizing with another ERM member radixin, whereas ezrin-T567A-iFLAG is cytoplasmic, and as reported recently, ezrin-T567E-iFLAG hyperlocalizes to the plasma membrane and localizes to the apical and basolateral domains of epithelial cells (Fig. 1*A*) (7).

As about 50% of the ezrin-iFLAG is phosphorylated *in vivo* (7), we were initially surprised to find that immunoprecipitation of ezrin-iFLAG failed to recover detectable EBP50. By contrast, the construct with an unmasked FERM domain due to the truncation of the final two residues, ezrin(1–583)-iFLAG, recovered EBP50 efficiently (Fig. 1*B*). To see if the interaction of EBP50 with ezrin-iFLAG can be stabilized, we explored the use of the reversible cross-linking reagent DSP. Cells were subjected to different concentrations of cross-linker for 2 min, and the recovery of EBP50 with ezrin-iFLAG was monitored. These results showed that brief cross-linking with 1.25 mM DSP allowed for modest recovery of EBP50 with ezrin-iFLAG and vice versa (Fig. 1*B*). To explore how the ezrin/EBP50 interaction was affected by ezrin Thr-567 phosphosite mutations, we detected EBP50 in unphosphorylatable ezrin-T567A-iFLAG or phosphomimetic ezrin-T567E-iFLAG immunoprecipitations (Fig. 1*C*). The modest recovery of EBP50 was significantly reduced by mutation to T567A but was unaffected by mutation to T567E (Fig. 1*C*). We obtained similar results by immunoprecipitating EBP50 and detecting ezrin-iFLAG phosphomutants (Fig. 1*D*). Thus, the DSP-preserved interaction between EBP50 and ezrin is dependent on the availability of Thr-567 for phos-

TABLE 1
Reported ERM-interacting proteins

Interaction partner	Selected refs.	Proposed binding mode	Proposed function
Aquaporin-0	50	Unknown	Unknown
ARHGAP-18/conundrum	33	FERM domain	Active RhoA level
Bitesize	51	FERM domain (lobe F3)	Adherens junction morphology
CD146	52	Unknown	Melanoma cell line migration through control of ERM-RhoGDI interaction
CD43	20, 53–56	FERM domain	Lymphocyte migration via PKC-mediated phosphorylation of CD43 tail; tethering of ERMs to plasma membrane for microvillus formation
CD44	9, 20, 53, 57–62	FERM domain	Migration speed and directionality; lymphocyte polarization; microvilli length and number
CLIC3/4/5	32, 42	C-terminal region of ezrin	Microvillus formation in RPE cells (CLIC4)
Dbl	48, 63–67	FERM domain with Dbl PH	Active Cdc42 level
DCC	68, 69	FERM domain	Netrin-induced axon guidance
Dlg1	70, 71	FERM domain	Immune synapse formation
SLC9A3R1/2 (EBP50/E3KARP)	17, 18, 21, 28, 30, 49, 72	FERM domain	Microvilli formation; clustering of various receptors
Eps8/−L1a	73	Coiled-coil domain NP*X*Y motif with Eps8 SH3	Microvillus length and spacing
Fes	74	Coiled-coil domain NP*X*Y motif with Fes SH3	Cell spreading and migration in response to HGF
ICAM-1/-2/-3	24, 25, 75–79	FERM domain	Polarization of ICAMs to the uropod in migrating lymphocytes; microvilli length and number
L1CAM	80, 81	FERM domain	Neurite outgrowth
Myo18aα	82	Unknown	Unknown
NHE-1	83, 84	FERM domain	Migration speed and directionality
NHE-3	85	FERM domain	NHE-3 surface distribution in OK cells
SCYL3/PACE-1	34	C-terminal region of ezrin	Unknown
Palladin	86, 87	Ezrin (278–585) with palladin Ig2/3	Unknown
PDZD8	88	Unknown	Glutamylated microtubule abundance and HSV-1 viral entry
PLEKHG6	89	FERM domain with PLEKHG6 C-terminal region	Macropinocytosis
Podocalyxin	90	Unknown	Unknown
PSGL-1	78, 91–95	FERM domain	Lymphocyte rolling on P-selectin
Rab11	96	Unknown	Collective cell migration
Ras	97	FERM domain	Active Ras level
RhoGDI	9, 66, 98	FERM domain	Active Rho GTPase level
S100P	99, 100	FERM domain	Cellular calcium response
SAP97	101	Unknown	Unknown
SOS	97	FERM domain with SOS DH/PH	Active Ras level
SYND2/Syndecan-2	35, 36	FERM domain	Unknown
Vps11/HOPS	102	Coiled-coil domain	Endocytosis
WWOX	103	Coiled-coil domain NP*X*Y motif with WWOX SH3	Secretion in gastric parietal cells
WWP-1	104	Coiled-coil domain NP*X*Y motif with WWP-1 SH3	Cell migration in response to HGF
ZAP-70	55	Unknown	Immune synapse formation
ITGB4/β4 integrin	105	FERM domain	β4 integrin protein level
DAG1/β-Dystroglycan	41, 48	FERM domain	Filopodia formation in C2C12 cells co-transfected with active Cdc42

phorylation and can be greatly increased by fully unmasking the FERM domain of ezrin as in ezrin-(1–583)-iFLAG (Fig. 1*C*).

Use of SILAC-Mass Spectrometry to Identify the Ezrin Interactome—To use mass spectrometry to identify proteins other than EBP50 that bind to wild-type ezrin, the ezrin-iFLAG cells were subject to SILAC relative to a reference culture expressing just the empty vector control. The control cells were grown in light medium, and the cells expressing ezrin-iFLAG were grown for sufficient time in heavy medium containing [^{13}C/^{15}N]arginine and [^{13}C/^{15}N]lysine to uniformly label all proteins. Both samples were subject to DSP cross-linking followed by FLAG immunoprecipitation. The immunoprecipitates were combined and trypsin-digested, and the digest was subjected to quantitative mass spectrometry. By comparing the abundance of specific peptides between the reference and ezrin-iFLAG samples, background material can be minimized and proteins enriched in the ezrin-iFLAG sample identified (Fig. 2*A*).

In each mass spectrometry run, 7,000–13,000 high confidence peptides (representing 2,000–3,500 unique proteins) were detected with most binding the FLAG antibody beads as background. To identify ezrin-iFLAG-bound proteins, we computationally selected those present at a heavy/light or "Xpress" ratio of greater than 3.6:1, and then to ensure reproducibility, we further selected only those that were detected in wild-type ezrin-iFLAG immunoprecipitations in at least 5/6 mass spectrometry experiments (biological replicates). These were considered as true interactors (Fig. 2*B*; supplemental Table 1). Of the 38 reproducibly interacting proteins, 9 were expected as either these proteins or their orthologs had been previously implicated in binding ERMs. These included the other ERM protein in these cells, radixin ("RDX," see Ref. 31), EBP50 (28), the chloride ion channel-like proteins CLIC3 and CLIC4 (32), the *Drosophila* ortholog of RhoA GTPase-activating protein Conundrum, ARHGAP18 (33), the pseudokinase SCYL3 (34), and syndecan-4 ("SDC4"), an adhesion molecule that contains the minimal syndecan ERM-binding motif first identified in syndecan-2 (35, 36). Additionally, the kinases LOK and SLK were identified, which were shown to be the major C-terminal threonine kinases for ERMs in *Drosophila* and

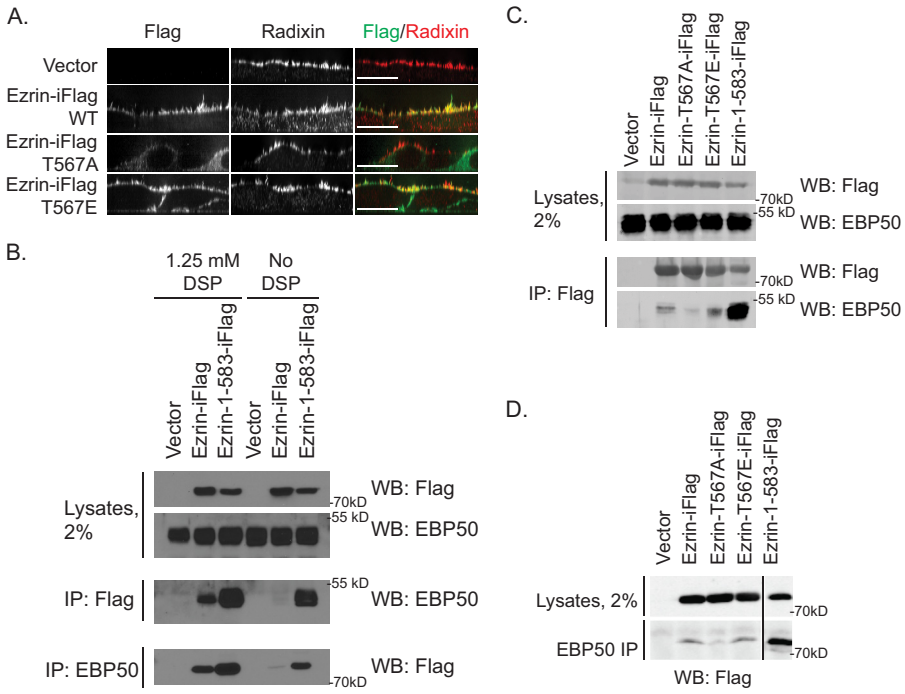

FIGURE 1. **Ezrin/EBP50 interaction can be preserved by enhancing the open state of ezrin or by DSP cross-linking.** *A,* Jeg-3 cells stably expressing the indicated ezrin-iFLAG variant were subjected to immunofluorescence to detect transfected FLAG-tagged ezrin and endogenous radixin, the other ERM protein present in this cell line. *Scale bar,* 10 μm. *B,* stable cell lines expressing empty vector control, ezrin-iFLAG, or hyperactive ezrin-iFLAG truncation 1–583 as indicated were subjected to immunoprecipitation (*IP*) with the indicated antibody with or without DSP pretreatment, and the immunoprecipitates were Western blotted (*WB*) for EBP50 or FLAG. *C,* stable cell lines expressing the indicated ezrin-iFLAG variant were subjected to DSP cross-linking followed by FLAG immunoprecipitation, and the immunoprecipitates were Western-blotted for EBP50. *D,* stable cell lines expressing the indicated ezrin-iFLAG variant were subjected to DSP cross-linking followed by EBP50 immunoprecipitation, and the immunoprecipitates were Western-blotted for FLAG.

mammalian epithelial and immune cells (7, 37–39). Consistent with ezrin localization at the plasma membrane and the nature of established interaction partners, 18/38 (47%) of the interaction partners were known or predicted to be transmembrane or membrane-associated proteins (supplemental Table 1).

Interactome of Phosphorylated Versus Unphosphorylated Ezrin—To identify which of these interactors bind preferentially to phosphorylated ezrin, we made use of SILAC comparing Jeg-3 cells expressing the nonphosphorylatable ezrin-T567A-iFLAG (labeled light) *versus* wild-type ezrin-iFLAG (*labeled heavy*; Fig. 3*A*). Because ezrin-iFLAG can be phosphorylated *in vivo*, this approach allowed us to identify proteins that selectively associate with active, phosphorylated ezrin and, conversely, ones that preferentially associate with inactive ezrin-T567A-iFLAG. The degree of enrichment for each candidate was normalized to the degree of enrichment of ezrin peptides. Biological replicates were performed, and correlation analysis confirmed that the enrichment statistics were reproducible (Fig. 3*B*). As another approach to identify proteins that distinguish the activity state of ezrin, we also undertook the SILAC procedure with cells expressing ezrin-iFLAG (labeled light), of which about 50% should be in the active state, and cells expressing ezrin-T567E-iFLAG (labeled heavy), a mimetic for the fully phosphorylated form. Again, correlation analysis between biological duplicates confirmed that enrichment statistics were reproducible (Fig. 3*C*). Moreover, most of the proteins identified in the two approaches were the same and were quite well correlated (Fig. 3*D*). The results of this analysis are presented in Fig. 3*E* (*left*), where a consensus of proteins (from these and subsequent experiments, listed by Uniprot identifier) that bind more active ezrin is shown on the *left*. These data reveal that binding of many interactors to ezrin was enhanced for wild-type *versus* ezrin-T567A, and approximately two-thirds of these were further enhanced by the phosphomimetic ezrin-T567E mutation. Among these proteins, as expected, is radixin (RDX), the other ERM protein present in these cells, EBP50 ("SLC9A3R1"), β-dystroglycan ("DAG1"), CLIC4, and the kinases LOK ("STK10") and SLK. In addition, about a dozen new proteins were identified.

We also identified a subclass of proteins that were recovered at approximately similar levels with inactive ezrin-T567A *versus* wild-type ezrin, yet they were more strongly identified as binding wild-type ezrin *versus* ezrin-T567E (Fig. 3*E*, *right*). We designated these proteins as interactors with closed ezrin. These include the F-actin nucleating formin FHOD-1, the Ras GTPase activating protein RASA1, and SCYL3 (also known as PACE-1 for protein-associating with the carboxyl-terminal domain of ezrin, see Ref. 34). We believe this is the first report of such proteins, which constitute a significant fraction of all ezrin-binding proteins.

Interactome Shows Enhanced Binding to Fully Unmasked Ezrin FERM Domain—The analysis above identified proteins that preferentially associate with phosphorylated *versus* unphosphorylated ezrin. In the current understanding of ezrin regulation, the phosphorylated form is regarded as fully active. However, it is clear from the results presented in Fig. 1 that EBP50 is much more efficiently recovered with an ezrin construct when the FERM domain is completely unmasked ezrin(1–583)-iFLAG, than

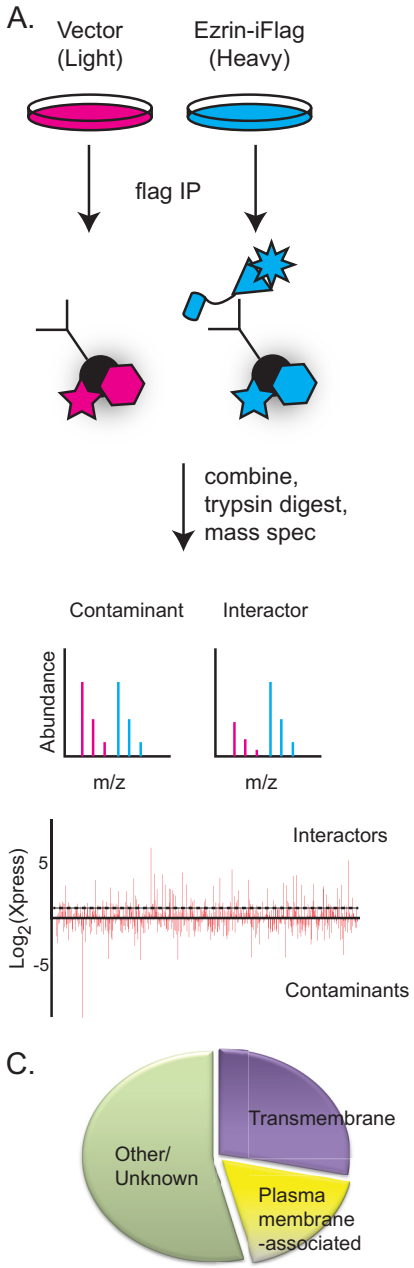

B.

Uniprot ID	Uniprot Description	Xpress Ratio, Ezrin-iFlag: Vec	Number of experiments observed	Number of peptides in 6 experiments	Reference for known or predicted interaction
CLIC4	Chloride intracellular channel protein 4	39.5	6/6	15	(32,42)
EZR	Ezrin	18.3	6/6	1974	
RDX	Radixin	14.1	6/6	201	
EGFR	Epidermal growth factor receptor	12.3	5/6	38	
FHOD1	FH1/FH2 domain-containing protein 1	11.9	6/6	209	
ITGA6	Integrin alpha-6	10.9	6/6	82	
SLC1A5	Neutral amino acid transporter B(0)	10.6	6/6	37	
TACSTD2	Tumor-associated calcium signal transducer 2	9.3	6/6	31	
UCK2	Uridine-cytidine kinase 2	8.5	6/6	15	
SDC4	Syndecan-4	7.9	5/6	14	(35,36)
RASA1	Ras GTPase-activating protein 1	7.8	5/6	45	
DAG1	Dystroglycan	7.8	6/6	51	(41,48)
REEP5	Receptor expression-enhancing protein 5	7.8	5/6	23	
BASP1	Brain acid soluble protein 1	7.4	5/6	16	
UCKL1	Uridine-cytidine kinase-like 1	6.9	6/6	48	
SLC9A3R1	Na(+)/H(+) exchange regulatory cofactor NHE-RF1	6.7	6/6	87	(15,18,21,26,28, 30,49,72)
EPCAM	Epithelial cell adhesion molecule	6.7	5/6	14	
BCR	Breakpoint cluster region protein	6.6	6/6	74	
ARHGAP18	Rho GTPase-activating protein 18	6.4	6/6	26	(33)
SCYL3	Protein-associating with the carboxyl-terminal domain of ezrin	6.4	6/6	34	(34)
SLC4A7	Sodium bicarbonate cotransporter 3	6.3	5/6	26	
MYO9B	Unconventional myosin-IXb	6.1	6/6	112	
SERPINB6	Serpin B6	5.9	6/6	17	
PACSIN3	Protein kinase C and casein kinase substrate in neurons protein 3	5.7	6/6	16	
ITGB1	Integrin beta-1	5.6	6/6	31	
ATP11C	Probable phospholipid-transporting ATPase IG	5.5	6/6	39	
UPRT	Uracil phosphoribosyltransferase	5.4	6/6	23	
GAN	Gigaxonin	5.3	6/6	20	
PPIP5K2	Inositol hexakisphosphate and diphosphoinositol-pentakisphosphate kinase 2	4.7	5/6	25	
LDHA/B	L-lactate dehydrogenase	4.7	6/6	163	
F11R	Junctional adhesion molecule A	4.4	6/6	36	
NUP93	Nuclear pore complex protein Nup93	4.2	6/6	66	
CLIC3	Chloride intracellular channel protein 3	4.2	6/6	72	(32)
STK10	Serine/threonine-protein kinase 10	4.2	6/6	51	(7,39)
PGAM1	Phosphoglycerate mutase 1	4.0	6/6	24	
UBXN1	UBX domain-containing protein 1	3.9	6/6	17	
SLK	STE20-like serine/threonine-protein kinase	3.8	6/6	27	(7)
FAM129B	Niban-like protein 1	3.6	5/6	30	

FIGURE 2. **Identification of 38 high confidence interactors of ezrin.** *A,* schematic of SILAC experiment. Jeg-3 cells stably transfected with vector control or expressing ezrin-iFLAG were differentially labeled in SILAC medium, independently subjected to cross-linking, and subjected to FLAG immunoprecipitation (*IP*). The immunoprecipitates were combined, trypsin-digested, and subjected to mass spectrometry, where heavy-to-light ratio was determined for each peptide. Diagram of mass spectrometry results for peptides from a typical background protein and an interactor is shown. Plot of the Xpress SILAC ratio for all recovered proteins (plotted along the *horizontal axis*) is shown. Proteins above the *dashed line* were considered interactors. (Most proteins enriched in the light sample are antibody fragments.) *B,* proteins with a heavy-to-light Xpress ratio greater than 3.6 for which 14 or more peptides were identified reproducibly in at least 5/6 experiments are listed. *C,* analysis of fraction of interactors containing transmembrane domains or shown to be membrane-associated (supplemental Table 1, columns U and V).

with either wild-type ezrin or ezrin-T567E. We therefore wanted to examine in an unbiased manner how general this type of interaction is.

We again performed SILAC to compare proteins recovered from cells expressing ezrin-iFLAG (light) with those recovered from cells expressing ezrin(1–583)-iFLAG (heavy). We found essentially the same set of proteins we did with ezrin-T567E-iFLAG but with a stronger preference for ezrin(1–583)-iFLAG (Fig. 3*F*). A notable exception was EBP50, being vastly more efficiently recovered with ezrin(1–583)-iFLAG, which is discussed further below.

Biochemical and Localization Validation of the Mass Spectrometry Results—Our proteomics approach identified three classes of ezrin interactors as follows: those that had a preference for phosphorylated ezrin (and ezrin-T567E), EBP50 (SLC9A3R1), which is recovered much more efficiently on unmasked ezrin than with phosphorylated ezrin, and an unexpected group of proteins that bind preferentially to inactive

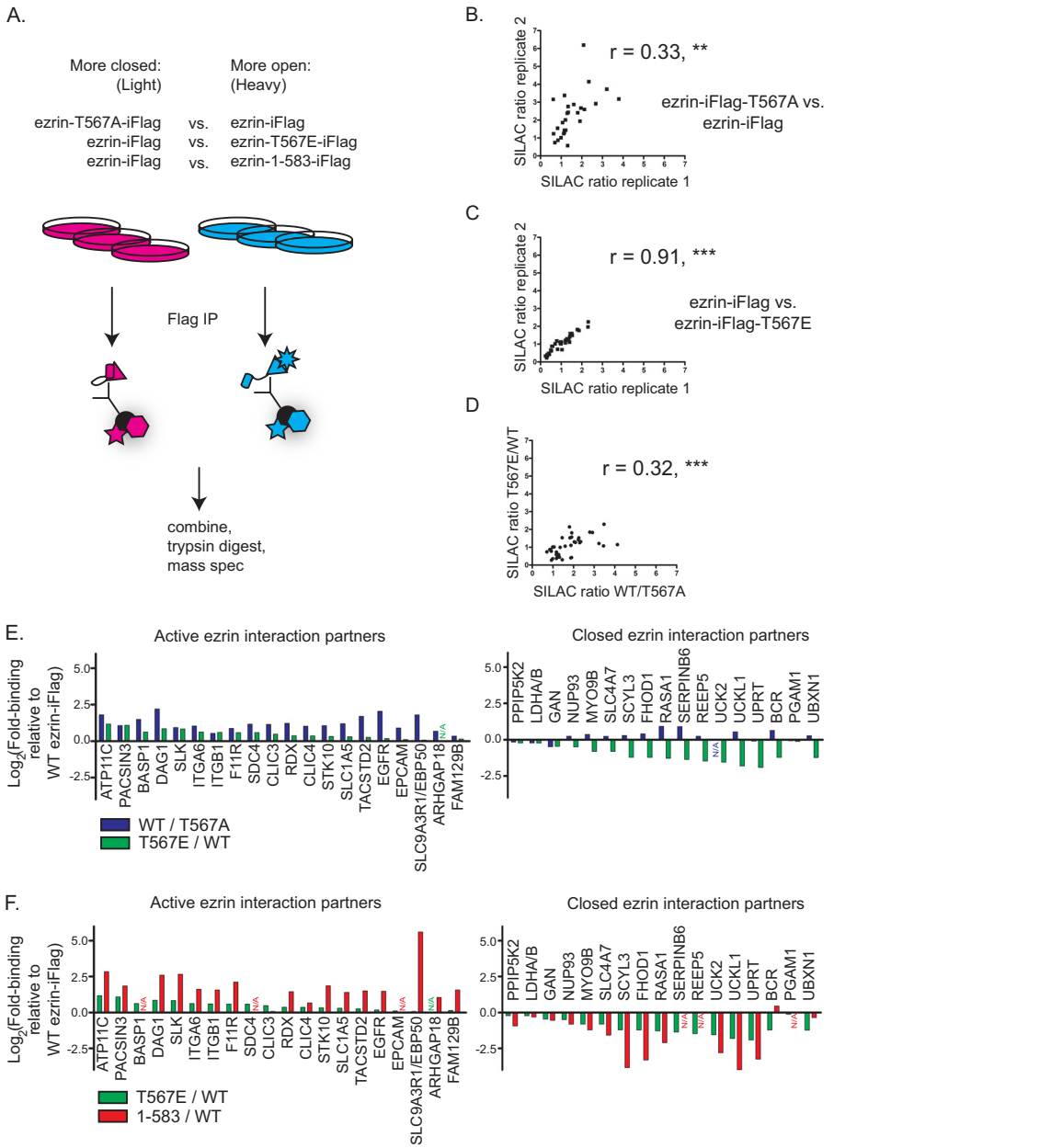

FIGURE 3. **Comparison of phosphorylated *versus* unphosphorylated ezrin interactome.** *A,* schematic of SILAC experiment. Jeg-3 cells transfected to express the indicated ezrin-iFLAG variant were differentially labeled in SILAC medium and independently subjected to cross-linking immunoprecipitation (*IP*). The immunoprecipitates were combined, trypsin-digested, and subjected to mass spectrometry (*spec*), where heavy-to-light ratio was determined for each peptide. *B* and *C,* correlation analysis between two biological replicates of the indicated SILAC experiment showing reproducible SILAC quantification. **, $p < 0.01$; ***, $p < 0.001$. *D,* correlation analysis between the average Xpress ratios from indicated SILAC comparisons showing that interactors preferring wild-type ezrin to unphosphorylatable ezrin tend to also prefer constitutively phosphorylated ezrin over wild type. ***, $p < 0.001$. *E, graph* of average Xpress ratio in indicated SILAC experiment by ezrin interactor. Based on their preference for ezrin-T567E-iFLAG over wild-type ezrin-iFLAG, proteins were classed as either interactors of active ezrin or closed ezrin. *F, graph* of average Xpress ratio in T567E *versus* wild-type as compared with 1–583 *versus* wild type for each ezrin interactor. For the 1–583 truncation, the preference of active ezrin interactor is further enhanced, although the preference of closed ezrin interactors is further decreased.

ezrin-T567A. To see if these classes of interactors could be confirmed by analysis of selected candidates, we immunoprecipitated ezrin from cells expressing the different variants and then Western-blotted for specific binding partners.

A close correspondence with the mass spectrometry data was found for EBP50 (SLC9A3R1), DAG1, and FHOD1 (FH1/FH2 domain-containing protein 1, a formin protein, see Fig. 4*A*). As we do not have reagents to test most of the other identified interactors, we expressed tagged versions in Jeg-3 cells and examined their recovery with co-expressed ezrin-iFLAG variants. For example, TACSTD2-myc shows a similar pattern of recovery as was found with the proteomics analysis (Fig. 4*B*). We summarize the results of this analysis in Fig. 4*C*.

We were surprised to recover a formin with ezrin, so we examined whether the interaction was affected by its interaction state. Many formins are negatively regulated by a head-to-tail intramolecular interaction involving a region known as the diaphanous association domain (DAD) (40). Equivalent

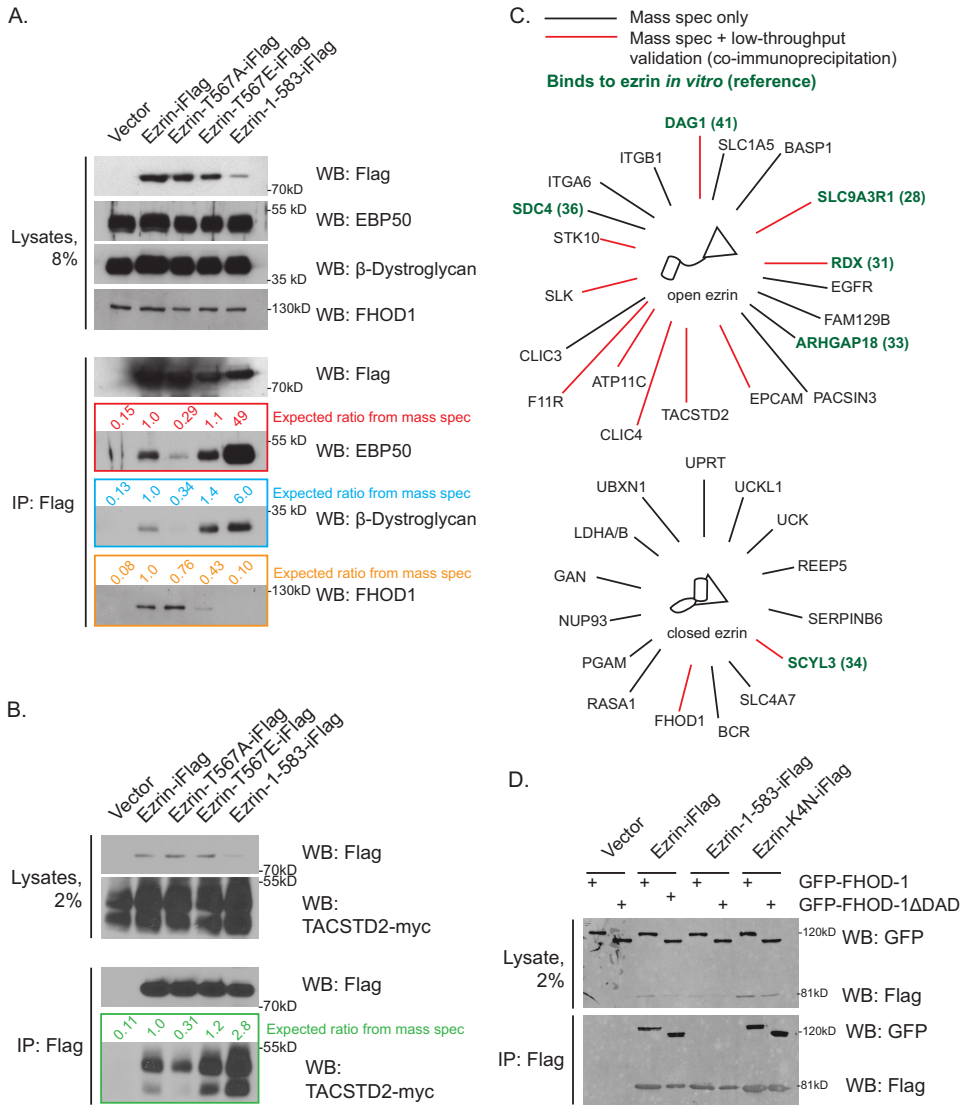

FIGURE 4. **Biochemical validation of SILAC experiments.** *A,* stable cell lines expressing empty vector control or indicated ezrin-iFLAG variants were subjected to cross-linking FLAG immunoprecipitation (*IP*) followed by Western blot (*WB*) for the indicated interactor. Predicted yield relative to wild-type ezrin-iFLAG is computed from mass spectrometry (*spec*) data in supplemental Table 1. *B,* parental Jeg-3 cell line was co-transfected to express empty vector or indicated ezrin-iFLAG variant along with TACSTD2-myc and then subjected to cross-linking FLAG immunoprecipitation and Myc Western blot. Predicted yield relative to wild-type ezrin-iFLAG is computed from mass spectrometry data in supplemental Table 1. *C,* summary of mass spectrometry interactors confirmed in low throughput methods. *Black lines* indicate proteins recovered in mass spectrometry only; *red lines* indicate proteins that were recovered and confirmed through low throughput co-immunoprecipitation followed by Western blotting experiments. *Green text* highlights proteins expected to bind directly with ERM proteins *in vitro* by others. *D,* cells transiently transfected to express empty vector or indicated ezrin-iFLAG variant and co-transfected to express full-length or hyperactivated (ΔDAD) GFP-FHOD-1 were subjected to FLAG immunoprecipitation, and the immunoprecipitates were resolved and Western-blotted for FLAG and GFP. FHOD-1 binds to wild-type or closed ezrin but not truncated and hyperactivated ezrin. The K4N mutant (K253N,K254N,K262N,K263N) of ezrin is completely closed in cells due a mutation in basic residues that bind to membrane PI(4,5)P_2 (10, 22).

amounts of GFP-FHOD1 or GFP-FHOD1ΔDAD (lacking the DAD domain) were selectively recovered with inactive forms of ezrin, indicating no preference for the activity state of the formin. No interaction was found with hyperactive ezrin(1–583)-iFLAG (Fig. 4*D*).

Another avenue to test the validity of the proteomic analysis is based on subcellular localization. Because active ezrin is found specifically in microvilli, candidates that show a preference for active ezrin might be expected to be enriched in microvilli. Conversely, those proteins that show a preference for inactive ezrin might be expected to be found predominantly in the cytoplasm, like ezrin-T567A-iFLAG (Fig. 1*A*).

The proteins DAG1 and CLIC4 have been shown previously to localize in microvilli (32, 41–43), so these serve as positive controls. Indeed, endogenous β-dystroglycan and transiently expressed GFP-CLIC4 both co-localize precisely with ezrin in the apical microvilli of Jeg-3 cells in maximum intensity projections through the entire cell or projections through a cross-section (Fig. 5, *A* and *B*). We then tested some of the other candidates, and as predicted, TACSTD2-myc, BASP1-GFP, and SLC1A5-GFP were all preferentially localized in microvilli (Fig. 5, *C–E*). Expression of proteins showing a preference for inactive ezrin, SCYL3-myc, and GFP-FHOD1 was not enriched in microvilli but was found diffusely in the cytoplasm or

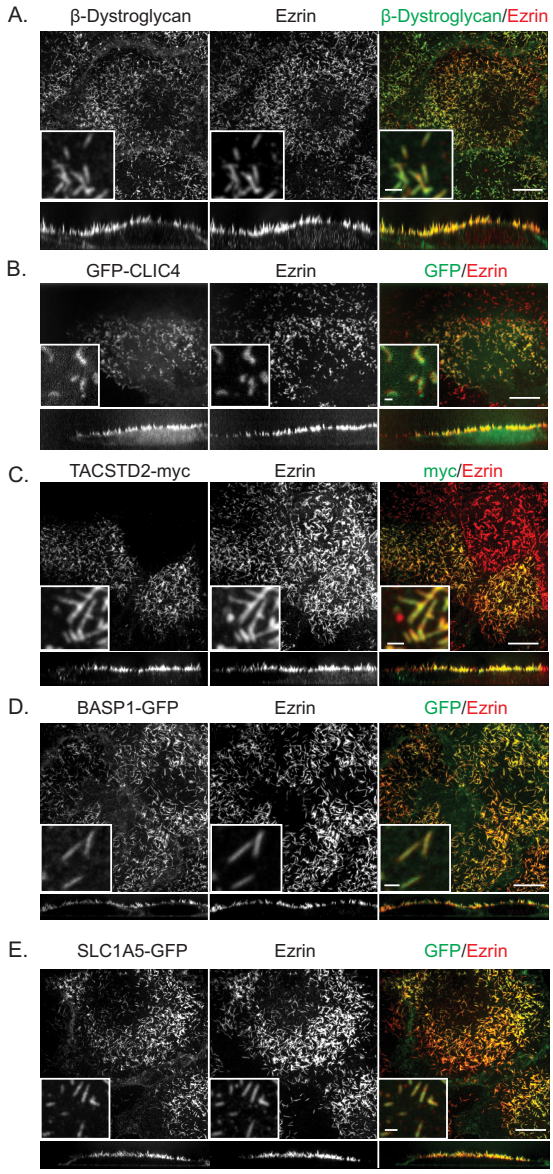

H.

Active ezrin interactors

Closed ezrin interactors

Protein	Microvilli	Basolateral Membranes	Other
ATP11C	+	+	+
BASP1	+++	+	
DAG1	+++	+/-	-
SLK	++	+	+
F11R	+	++	+
RDX	+++	-	-
CLIC4	+++	+/-	-
STK10	++	+	+
SLC1A5	+++	+	+
TACSTD2	+++	+/-	+
EPCAM	+	+++	-
SLC9A3R1	+++	-	-
ARHGAP18	+	+	++
FAM129B	+/-	+++	+
SCYL3	+/-	+/-	+++
FHOD1	-	++	+++

FIGURE 5. **Active ezrin interactors localize in microvilli, whereas closed ezrin interactors localize in the cytoplasm.** *A–G,* maximum intensity (*XY*) projection, 10-fold magnified image, and side view (*XZ*) of cells stained for endogenous β-dystroglycan (*A*) or transfected to express the indicated tagged interactor and counterstained for ezrin. Selected active ezrin interactors (*A–E*) localize in the microvilli. *F* and *G,* two interactors of closed ezrin do not localize to microvilli but are found in the cytoplasm. *Scale bars* are 10 μm for full maximum intensity projections and side views and 1 μm for *insets*. Side views have been stretched vertically 3-fold for clarity. *H,* summary of localization of all interactors examined.

enriched on basolateral membranes (Fig. 5, *F* and *G*). A summary of all the candidates examined is shown in Fig. 5*H*. Thus, both the co-immunoprecipitation and localization results strongly support the proteomic data.

Function of Novel Ezrin Interaction Partners—Ezrin is known to interact with many proteins (Table 1), and in this study we have documented yet more. Ezrin is important for the presence of microvilli on Jeg-3 cells (7), so we asked if altering the expression of ezrin-interacting proteins had any effect on microvilli.

Jeg-3 epithelial cells express both ezrin and radixin. When ezrin levels are reduced 80% by siRNA treatment, about half the cells lose microvilli. The number of cells with microvilli can be further reduced to 20% by simultaneously knocking down radixin, supporting a critical role for ERM proteins in maintaining microvilli in Jeg-3 cells (Fig, 6, *A* and *B*). We next tested the effect of knocking down two of our candidates, DAG1 and TACSTD2. Both endogenous proteins were found to localize in microvilli (Figs. 5*A* and 6*C*). Although reduction of the levels of β-dystroglycan has no discernible effect, reduction of TACSTD2 reduced the number of cells with microvilli modestly (Fig. 6, *D–F*).

The overexpression of activated ERM proteins or ERM-binding proteins in fibroblastic cells has been shown to cause an increase in the number of microvilli-like structures (MLSs) (20, 44). We therefore examined the effect of overexpression of our candidates, DAG1, TACSTD2, BASP1, and ATP11C (which must be co-overexpressed with its chaperone Cdc50A for plasma membrane enrichment, see Ref. 27), and CLIC4 in COS7 fibroblastic cells. Overexpression of wild-type or activated ezrin but not the more closed ezrin mutant, T567A,

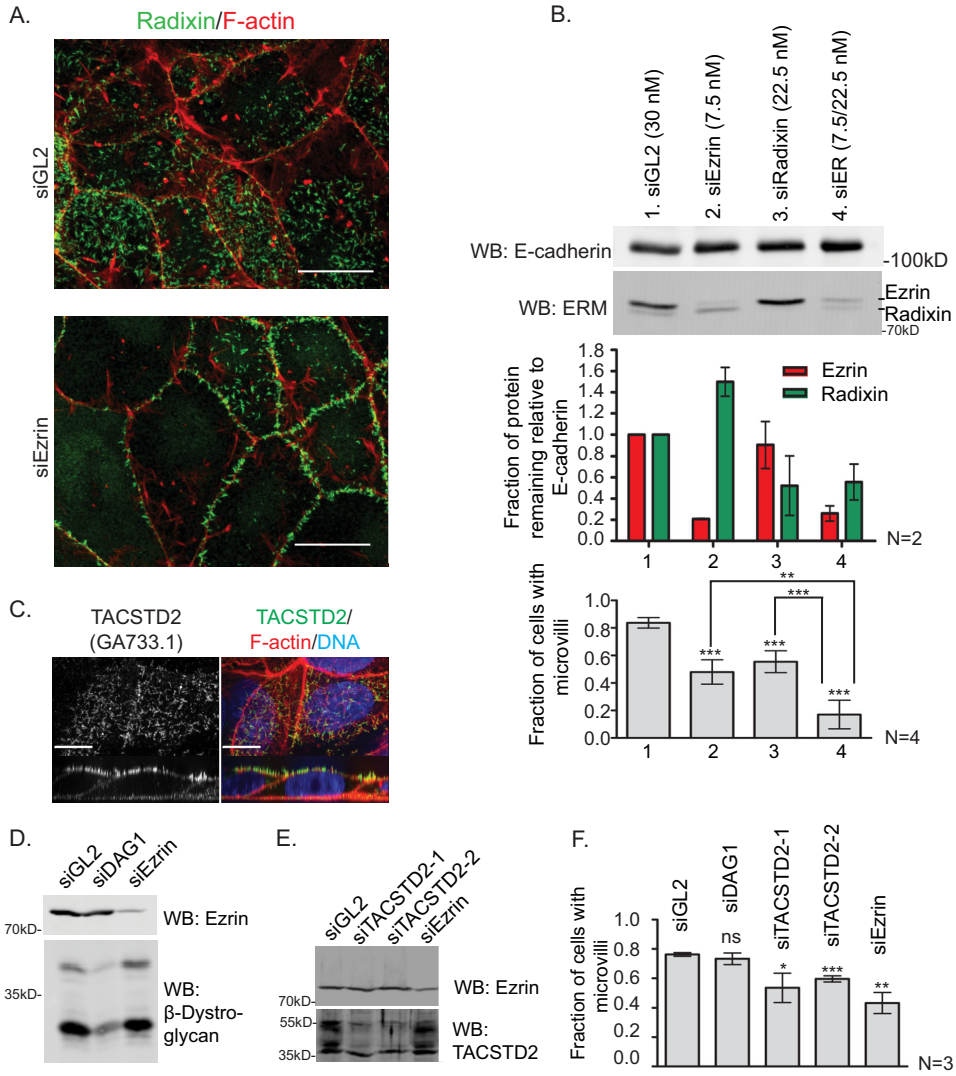

FIGURE 6. **TACSTD2 suppression by RNA interference results in a moderate loss-of-microvilli phenotype.** *A,* Jeg-3 cells were transfected with nontargeting control siRNA (*siGL2*) or ezrin siRNA (*siEzrin*) for 72 h and then stained for F-actin and radixin to reveal a loss of microvilli after to ezrin knockdown. *Scale bars,* 10 μm. *B,* Jeg-3 cells were transfected with indicated siRNAs for 72 h, and cell lysates were prepared and Western-blotted (*WB*) for ezrin and radixin. The remaining protein was quantified. The cells were also fixed and stained for F-actin, β-dystroglycan, and EBP50 (data not shown). The presence of microvilli by any of these markers was scored using a previously described scheme (7, 15, 17, 18, 49). *Error bars* are standard deviation. *p* values were computed using a two-tailed *t* test. *, $p < 0.05$; **, $p < 0.01$; ***, $p < 0.001$; *ns*, not significant. *C,* endogenous TACSTD2 was detected by immunofluorescence using the GA733.1 antibody. *Scale bars,* 10 μm. *D* and *E,* cells were transfected with indicated siRNA for 72 h, then lysates were prepared and Western-blotted (*WB*) as indicated. *F,* Jeg-3 cells transfected as described in *B* were stained for radixin, and the presence of microvilli was scored as in *B*. *Error bars* are standard deviation. *p* values were computed using a two-tailed *t* test. *, $p < 0.05$; **, $p < 0.01$, ***; $p < 0.001$; *ns*, not significant.

caused an elevation in the percentage of cells containing MLSs as indicated by F-actin and moesin staining (data not shown) as expected (quantified in Fig. 7*B*). Like moesin, ezrin was also enriched in these structures (data not shown). In the case of our candidates, DAG1, TACSTD2, and CLIC4 each caused an elevation in the percentage of cells containing MLSs (Fig. 7, *A* and *B*). By contrast, the overexpression of DAG1ΔE, a mutant previously shown to be incapable of binding to ezrin (41), BASP1, or ATP11C (expressed with its chaperone as above) had no effect (Fig. 7*B*). Western blotting showed that each transfected protein was present at the expected size (Fig. 7*C*). The combined analysis suggests that some of our interactors are capable of promoting the formation of dorsal microvilli-like structures in fibroblastic cells. Taken together with our knockdown experiments, we propose that ezrin anchorage to the plasma membrane is likely due to the concerted activity of many binding partners.

DISCUSSION

ERMs function as regulated linking proteins, so to learn more about them, we took a global proteomics view, not only to uncover new ligands and regulators but also to understand the role of conformational change in ERM function.

Our use of cross-linking immunoprecipitation rather than a direct interaction assay, as reported previously (28), biased the analysis toward proteins bound to ezrin *in vivo*, including transient interactors, rather than those with tenacious *in vitro* affinity. This revealed many new interactors. We provide three validations of our approach as follows: 1) greater than one-quarter of the interactors were expected based on previous studies, and

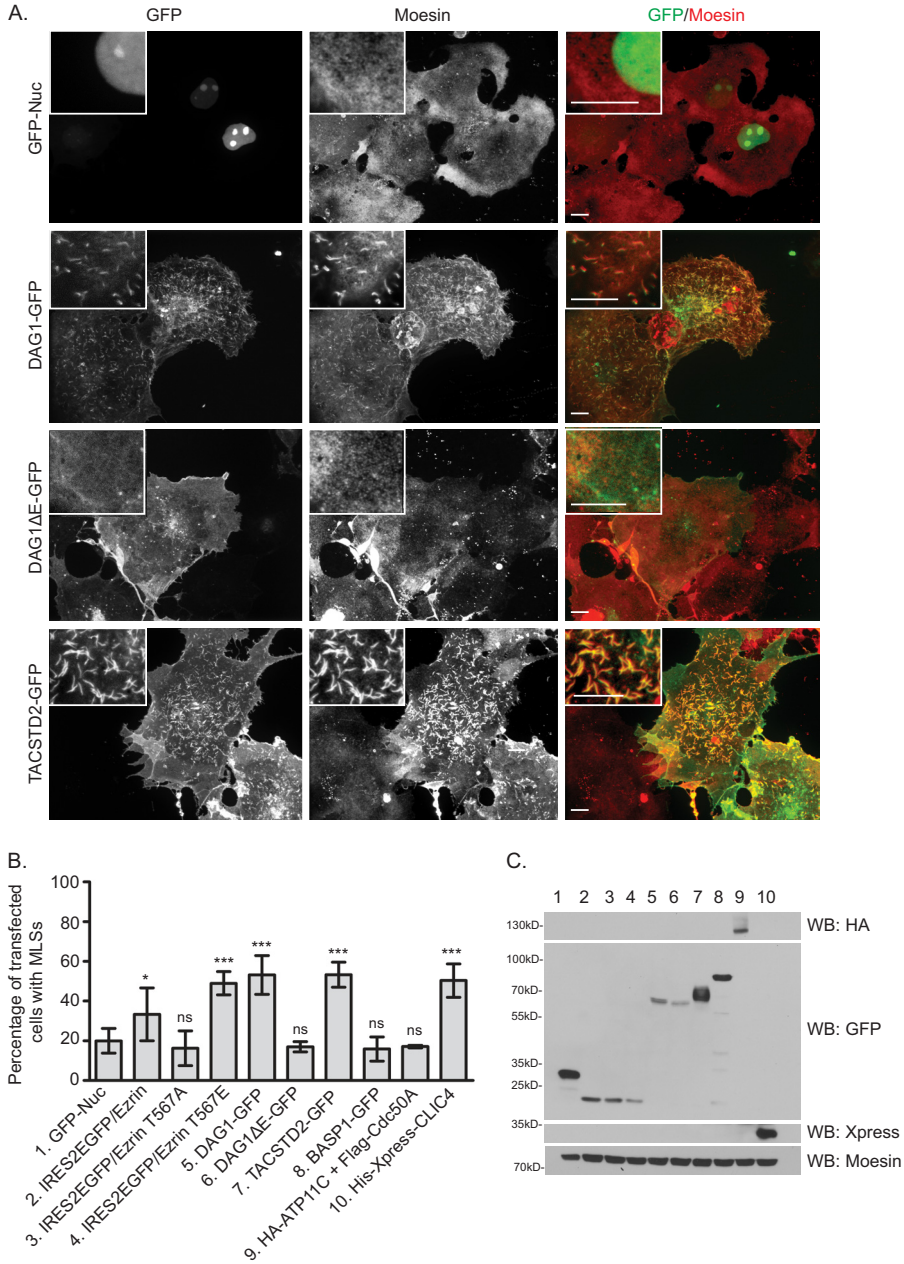

FIGURE 7. **DAG1, TACSTD2, or CLIC4 overexpression in fibroblastic cells promotes dorsal ERM-containing surface structures.** *A,* COS7 fibroblastic cells were transfected with indicated protein and stained for endogenous moesin (an ERM protein present in these cells). *Panels*, maximum intensity projections through a field of cells; *insets*, maximum intensity projections through a small dorsal region of one transfected cell. *Bar,* 10 μm. *B,* cells transfected as in *A* were scored for the presence of MLSs. *GFP-Nuc* is nuclear-localized GFP, intended as a negative-control. IRES2EGFP allows expression of free GFP as a reporter of untagged ezrin construct transfection. *Error bars* are standard deviation. *p* values were computed using a two-tailed *t* test. *, $p < 0.05$; ***; $p < 0.001$; *ns*, not significant. *C,* cells expressing the transfected proteins as listed in *B* were subjected to Western blotting (*WB*) with indicated antibodies.

a large fraction (almost half) of the interactors contained transmembrane helices or membrane-binding domains; 2) where tested, we were able to biochemically validate the mass spectrometry results; 3) many of the interactors, including three novel interactors, accumulate not just on the plasma membrane, but also strongly in microvilli.

Our analysis defined three conformational states of ezrin (closed, active, and fully open) as perceived by the 38 high confidence interactors. One group, designated as active ezrin interactors, bound more to wild-type than unphosphorylatable T567A ezrin, more to phosphomimetic T567E than wild-type ezrin, and more to truncated 1–583 than T567E ezrin. A second group, closed ezrin interactors, bound roughly equally to wild-type and T567A ezrin, less to T567E ezrin, and still less to 1–583 ezrin. Most ERM-binding proteins had a modest (1.2–4.2-fold) preference for truncated 1–583 ezrin over phosphomimetic T567E ezrin. However, EBP50, which binds to the FERM domain more intimately than other known FERM interaction partners (21), was unique in having an extreme (45-fold) preference for 1–583 ezrin over T567E ezrin. This result supports *in vitro* data that, even when phosphorylated, the tail of ezrin still serves as a potent competitive inhibitor of FERM

domain accessibility (16). Moreover, it argues that the influence of the tail on FERM domain binding differs in degree for different interaction partners and highlights the uniqueness of EBP50's interaction with ezrin.

Surprisingly, we identified multiple partners of the inactive state of ezrin. As expected, these are not enriched in microvilli but are found in the cytoplasm. To date, the only known interactor of inactive ezrin is the lipid $PI(4,5)P_2$, which plays a role in the transition to an activated state. Thus, we are looking into the function of this large class of ezrin interactors in ezrin regulation.

The conformational activation model (45) stipulates that interactors binding ezrin on the plasma membrane should bind preferentially to more open forms of ezrin. Consistently, most interactors containing transmembrane helices were active ezrin interactors. But is this merely an effect of the localization of open *versus* closed ezrin? We can determine this by comparing the binding partners of the two constitutively open forms of ezrin, truncated ezrin(1–583)-iFLAG *versus* phosphomimetic ezrin-T567E-iFLAG, because both localize identically in a depolarized manner on the plasma membrane (7). Strikingly, all but one transmembrane interactor (8/9) bound truncated ezrin(1–583)-iFLAG to a greater extent than phosphomimetic ezrin-T567E-iFLAG (for instance, see TACSTD2, Fig. 5*B*). Therefore, we argue that the extent to which an interactor binds to ezrin is not only a function of the localization of the proteins but also ezrin conformation.

This work adds to several recent reports showing that protein complexes involving ERMs are unusually dynamic. Ezrin turns over from microvilli faster than microvilli themselves turnover (14, 15, 46), and EBP50 turns over even faster than ezrin (15). The turnover rate of EBP50 is regulated by PDZ interactions, and impairing these interactions decreases EBP50's turnover rate from microvilli and increases the recovery of co-immunoprecipitated ezrin (15). Moreover, cross-linking was also used to preserve the interactions between the *Drosophila* orthologs of ERMs, EBP50, and the LOK/SLK kinase (47). Thus, rapid turnover seems to be a general feature of ERM interactions.

Some known interactors were notably absent from our analysis, possibly reflecting cell type-specific expression differences. None of the peptides in our analysis corresponded to CD44, ICAM-2, ICAM-3, syndecan-2, CLIC5, and S100P (Table 1; data not shown). Thus, these are not major ezrin-associated proteins in Jeg-3 cells and may not be expressed. ICAM-1 is present in Jeg-3 cells but appeared in our immunoprecipitates in amounts too low to accurately quantify.

RNA interference knockdown of two of the top candidate ERM-binding transmembrane proteins in Jeg-3 epithelial cells failed to yield a striking phenotype, although TACSTD2 suppression partially reduced the number of microvilli-bearing cells in Jeg-3 cells (Fig. 6*F*), and dominant-negative β-dystroglycan (DAG1ΔE) inhibited the formation of active-Cdc42-induced filopodia in a myoblast cell line (41). Conversely, overexpression of TACSTD2, DAG1, or CLIC4 caused the enumeration of MLSs in overexpressing fibroblastic cells, which normally produce dorsal ERM-containing protrusions only rarely (Fig. 7). The lack of overt phenotype in the epithelial cell line can be interpreted in two ways as follows: 1) transmembrane ERM-binding proteins are not required as ERM tethering or clustering agents as has been proposed (20); 2) ERM binding to numerous transmembrane proteins coordinately regulates their tethering or clustering. In support of the second possibility, ERM-binding motifs are minimal and present in many transmembrane proteins, and the proteins containing them have evolved entirely separate functions (*e.g.* β-dystroglycan functions as a receptor for the extracellular matrix component laminin), making it possible that ERMs evolved promiscuous affinity to a wide range of available ligands. Also in support of this model, our calculations suggest that ezrin is stoichiometrically present in a similar abundance to actin (data not shown), suggesting that no one membrane protein is in sufficient abundance to bind all the ezrin molecules, such that many transmembrane proteins would be needed to serve such a function. Thus, our current efforts are to ask whether simultaneous perturbation of multiple transmembrane ezrin interactors described here affects ezrin function.

Acknowledgments—We are grateful to Dr. A. Hanono for the cross-linking immunoprecipitation protocol. We also thank Drs. D. Garbett, D. Lalonde, and C. Sauvanet for critically reading this manuscript. Dr. M. Berryman (Ohio University), Dr. R. Thorne (University of Newcastle), Dr. H. W. Shin (University of Kyoto), and Dr. U. Naik (University of Delaware) generously provided plasmids for this study. The CPCT-Ezrin-1 and CPCT-Moesin-1 antibodies were obtained from the Developmental Studies Hybridoma Bank developed under the auspices of the NICHD, National Institutes of Health, and maintained by the Department of Biology, University of Iowa, Iowa City.

REFERENCES

1. Bretscher, A. (1983) Purification of an 80,000-dalton protein that is a component of the isolated microvillus cytoskeleton, and its localization in nonmuscle cells. *J. Cell Biol.* **97,** 425–432
2. Fehon, R. G., McClatchey, A. I., and Bretscher, A. (2010) Organizing the cell cortex: the role of ERM proteins. *Nat. Rev. Mol. Cell Biol.* **11,** 276–287
3. Saotome, I., Curto, M., and McClatchey, A. I. (2004) Ezrin is essential for epithelial organization and villus morphogenesis in the developing intestine. *Dev. Cell* **6,** 855–864
4. Bonilha, V. L., Rayborn, M. E., Saotome, I., McClatchey, A. I., and Hollyfield, J. G. (2006) Microvilli defects in retinas of ezrin knockout mice. *Exp. Eye Res.* **82,** 720–729
5. Karagiosis, S. A., and Ready, D. F. (2004) Moesin contributes an essential structural role in *Drosophila* photoreceptor morphogenesis. *Development.* **131,** 725–732
6. Bonilha, V. L., Finnemann, S. C., and Rodriguez-Boulan, E. (1999) Ezrin promotes morphogenesis of apical microvilli and basal infoldings in retinal pigment epithelium. *J. Cell Biol.* **147,** 1533–1548
7. Viswanatha, R., Ohouo, P. Y., Smolka, M. B., and Bretscher, A. (2012) Local phosphocycling mediated by LOK/SLK restricts ezrin function to the apical aspect of epithelial cells. *J. Cell Biol.* **199,** 969–984
8. Fievet, B. T., Gautreau, A., Roy, C., Del Maestro, L., Mangeat, P., Louvard, D., and Arpin, M. (2004) Phosphoinositide binding and phosphorylation act sequentially in the activation mechanism of ezrin. *J. Cell Biol.* **164,** 653–659
9. Hirao, M., Sato, N., Kondo, T., Yonemura, S., Monden, M., Sasaki, T., Takai, Y., Tsukita, S., and Tsukita, S. (1996) Regulation mechanism of ERM (ezrin/radixin/moesin) protein/plasma membrane association: possible involvement of phosphatidylinositol turnover and Rho-dependent signaling pathway. *J. Cell Biol.* **135,** 37–51
10. Niggli, V., Andréoli, C., Roy, C., and Mangeat, P. (1995) Identification of

a phosphatidylinositol-4,5-bisphosphate-binding domain in the N-terminal region of ezrin. *FEBS Lett.* **376,** 172–176
11. Matsui, T., Yonemura, S., Tsukita, S., and Tsukita, S. (1999) Activation of ERM proteins *in vivo* by Rho involves phosphatidylinositol 4-phosphate 5-kinase and not ROCK kinases. *Curr. Biol.* **9,** 1259–1262
12. Yonemura, S., Matsui, T., Tsukita, S., and Tsukita, S. (2002) Rho-dependent and -independent activation mechanisms of ezrin/radixin/moesin proteins: an essential role for polyphosphoinositides *in vivo*. *J. Cell Sci.* **115,** 2569–2580
13. Gautreau, A., Louvard, D., and Arpin, M. (2000) Morphogenic effects of ezrin require a phosphorylation-induced transition from oligomers to monomers at the plasma membrane. *J. Cell Biol.* **150,** 193–203
14. Coscoy, S., Waharte, F., Gautreau, A., Martin, M., Louvard, D., Mangeat, P., Arpin, M., and Amblard, F. (2002) Molecular analysis of microscopic ezrin dynamics by two-photon FRAP. *Proc. Natl. Acad. Sci. U.S.A.* **99,** 12813–12818
15. Garbett, D., and Bretscher, A. (2012) PDZ interactions regulate rapid turnover of the scaffolding protein EBP50 in microvilli. *J. Cell Biol.* **198,** 195–203
16. Chambers, D. N., and Bretscher, A. (2005) Ezrin mutants affecting dimerization and activation. *Biochemistry* **44,** 3926–3932
17. Hanono, A., Garbett, D., Reczek, D., Chambers, D. N., and Bretscher, A. (2006) EPI64 regulates microvillar subdomains and structure. *J. Cell Biol.* **175,** 803–813
18. Garbett, D., LaLonde, D. P., and Bretscher, A. (2010) The scaffolding protein EBP50 regulates microvillar assembly in a phosphorylation-dependent manner. *J. Cell Biol.* **191,** 397–413
19. Morales, F. C., Takahashi, Y., Kreimann, E. L., and Georgescu, M. M. (2004) Ezrin-radixin-moesin (ERM)-binding phosphoprotein 50 organizes ERM proteins at the apical membrane of polarized epithelia. *Proc. Natl. Acad. Sci. U.S.A.* **101,** 17705–17710
20. Yonemura, S., Tsukita, S., and Tsukita, S. (1999) Direct involvement of ezrin/radixin/moesin (ERM)-binding membrane proteins in the organization of microvilli in collaboration with activated ERM proteins. *J. Cell Biol.* **145,** 1497–1509
21. Finnerty, C. M., Chambers, D., Ingraffea, J., Faber, H. R., Karplus, P. A., and Bretscher, A. (2004) The EBP50-moesin interaction involves a binding site regulated by direct masking on the FERM domain. *J. Cell Sci.* **117,** 1547–1552
22. Barret, C., Roy, C., Montcourrier, P., Mangeat, P., and Niggli, V. (2000) Mutagenesis of the phosphatidylinositol 4,5-bisphosphate (PIP_2) binding site in the NH_2-terminal domain of ezrin correlates with its altered cellular distribution. *J. Cell Biol.* **151,** 1067–1080
23. Ben-Aissa, K., Patino-Lopez, G., Belkina, N. V., Maniti, O., Rosales, T., Hao, J. J., Kruhlak, M. J., Knutson, J. R., Picart, C., and Shaw, S. (2012) Activation of moesin, a protein that links actin cytoskeleton to the plasma membrane, occurs by phosphatidylinositol 4,5-bisphosphate (PIP_2) binding sequentially to two sites and releasing an autoinhibitory linker. *J. Biol. Chem.* **287,** 16311–16323
24. Hamada, K., Shimizu, T., Matsui, T., Tsukita, S., and Hakoshima, T. (2000) Structural basis of the membrane-targeting and unmasking mechanisms of the radixin FERM domain. *EMBO J.* **19,** 4449–4462
25. Hamada, K., Shimizu, T., Yonemura, S., Tsukita, S., Tsukita, S., and Hakoshima, T. (2003) Structural basis of adhesion-molecule recognition by ERM proteins revealed by the crystal structure of the radixin-ICAM-2 complex. *EMBO J.* **22,** 502–514
26. Terawaki, S., Maesaki, R., and Hakoshima, T. (2006) Structural basis for NHERF recognition by ERM proteins. *Structure* **14,** 777–789
27. Takatsu, H., Baba, K., Shima, T., Umino, H., Kato, U., Umeda, M., Nakayama, K., and Shin, H. W. (2011) ATP9B, a P4-ATPase (a putative aminophospholipid translocase), localizes to the trans-Golgi network in a CDC50 protein-independent manner. *J. Biol. Chem.* **286,** 38159–38167
28. Reczek, D., Berryman, M., and Bretscher, A. (1997) Identification of EBP50: A PDZ-containing phosphoprotein that associates with members of the ezrin-radixin-moesin family. *J. Cell Biol.* **139,** 169–179
29. Smolka, M. B., Albuquerque, C. P., Chen, S. H., and Zhou, H. (2007) Proteome-wide identification of *in vivo* targets of DNA damage checkpoint kinases. *Proc. Natl. Acad. Sci. U.S.A.* **104,** 10364–10369
30. Reczek, D., and Bretscher, A. (1998) The carboxyl-terminal region of EBP50 binds to a site in the amino-terminal domain of ezrin that is masked in the dormant molecule. *J. Biol. Chem.* **273,** 18452–18458
31. Gary, R., and Bretscher, A. (1993) Heterotypic and homotypic associations between ezrin and moesin, two putative membrane-cytoskeletal linking proteins. *Proc. Natl. Acad. Sci. U.S.A.* **90,** 10846–10850
32. Berryman, M., and Bretscher, A. (2000) Identification of a novel member of the chloride intracellular channel gene family (CLIC5) that associates with the actin cytoskeleton of placental microvilli. *Mol. Biol. Cell* **11,** 1509–1521
33. Neisch, A. L., Formstecher, E., and Fehon, R. G. (2013) Conundrum, an ARHGAP18 orthologue, regulates RhoA and proliferation through interactions with moesin. *Mol. Biol. Cell* **24,** 1420–1433
34. Sullivan, A., Uff, C. R., Isacke, C. M., and Thorne, R. F. (2003) PACE-1, a novel protein that interacts with the C-terminal domain of ezrin. *Exp. Cell Res.* **284,** 224–238
35. Granés, F., Urena, J. M., Rocamora, N., and Vilaró, S. (2000) Ezrin links syndecan-2 to the cytoskeleton. *J. Cell Sci.* **113,** 1267–1276
36. Granés, F., Berndt, C., Roy, C., Mangeat, P., Reina, M., and Vilaró, S. (2003) Identification of a novel ezrin-binding site in syndecan-2 cytoplasmic domain. *FEBS Lett.* **547,** 212–216
37. Hipfner, D. R., Keller, N., and Cohen, S. M. (2004) Slik Sterile-20 kinase regulates moesin activity to promote epithelial integrity during tissue growth. *Genes Dev.* **18,** 2243–2248
38. Hughes, S. C., and Fehon, R. G. (2006) Phosphorylation and activity of the tumor suppressor merlin and the ERM protein moesin are coordinately regulated by the Slik kinase. *J. Cell Biol.* **175,** 305–313
39. Belkina, N. V., Liu, Y., Hao, J. J., Karasuyama, H., and Shaw, S. (2009) LOK is a major ERM kinase in resting lymphocytes and regulates cytoskeletal rearrangement through ERM phosphorylation. *Proc. Natl. Acad. Sci. U.S.A.* **106,** 4707–4712
40. Alberts, A. S. (2001) Identification of a carboxyl-terminal diaphanous-related formin homology protein autoregulatory domain. *J. Biol. Chem.* **276,** 2824–2830
41. Spence, H. J., Chen, Y. J., Batchelor, C. L., Higginson, J. R., Suila, H., Carpen, O., and Winder, S. J. (2004) Ezrin-dependent regulation of the actin cytoskeleton by β-dystroglycan. *Hum. Mol. Genet.* **13,** 1657–1668
42. Chuang, J. Z., Chou, S. Y., and Sung, C. H. (2010) Chloride intracellular channel 4 is critical for the epithelial morphogenesis of RPE cells and retinal attachment. *Mol. Biol. Cell* **21,** 3017–3028
43. Berryman, M. A., and Goldenring, J. R. (2003) CLIC4 is enriched at cell-cell junctions and colocalizes with AKAP350 at the centrosome and midbody of cultured mammalian cells. *Cell Motil. Cytoskeleton* **56,** 159–172
44. Oshiro, N., Fukata, Y., and Kaibuchi, K. (1998) Phosphorylation of moesin by rho-associated kinase (Rho-kinase) plays a crucial role in the formation of microvilli-like structures. *J. Biol. Chem.* **273,** 34663–34666
45. Bretscher, A., Reczek, D., and Berryman, M. (1997) Ezrin: a protein requiring conformational activation to link microfilaments to the plasma membrane in the assembly of cell surface structures. *J. Cell Sci.* **110,** 3011–3018
46. Gorelik, J., Shevchuk, A. I., Frolenkov, G. I., Diakonov, I. A., Lab, M. J., Kros, C. J., Richardson, G. P., Vodyanoy, I., Edwards, C. R., Klenerman, D., and Korchev, Y. E. (2003) Dynamic assembly of surface structures in living cells. *Proc. Natl. Acad. Sci. U.S.A.* **100,** 5819–5822
47. Hughes, S. C., Formstecher, E., and Fehon, R. G. (2010) Sip1, the *Drosophila* orthologue of EBP50/NHERF1, functions with the sterile 20 family kinase Slik to regulate moesin activity. *J. Cell Sci.* **123,** 1099–1107
48. Batchelor, C. L., Higginson, J. R., Chen, Y. J., Vanni, C., Eva, A., and Winder, S. J. (2007) Recruitment of Dbl by ezrin and dystroglycan drives membrane proximal Cdc42 activation and filopodia formation. *Cell Cycle* **6,** 353–363
49. LaLonde, D. P., Garbett, D., and Bretscher, A. (2010) A regulated complex of the scaffolding proteins PDZK1 and EBP50 with ezrin contribute to microvillar organization. *Mol. Biol. Cell* **21,** 1519–1529
50. Wang, Z., and Schey, K. L. (2011) Aquaporin-0 interacts with the FERM domain of ezrin/radixin/moesin proteins in the ocular lens. *Invest. Ophthalmol. Vis. Sci.* **52,** 5079–5087
51. Pilot, F., Philippe, J. M., Lemmers, C., and Lecuit, T. (2006) Spatial con-

trol of actin organization at adherens junctions by a synaptotagmin-like protein Btsz. *Nature* **442,** 580–584
52. Luo, Y., Zheng, C., Zhang, J., Lu, D., Zhuang, J., Xing, S., Feng, J., Yang, D., and Yan, X. (2012) Recognition of CD146 as an ERM-binding protein offers novel mechanisms for melanoma cell migration. *Oncogene* **31,** 306–321
53. Yonemura, S., Hirao, M., Doi, Y., Takahashi, N., Kondo, T., Tsukita, S., and Tsukita, S. (1998) Ezrin/radixin/moesin (ERM) proteins bind to a positively charged amino acid cluster in the juxta-membrane cytoplasmic domain of CD44, CD43, and ICAM-2. *J. Cell Biol.* **140,** 885–895
54. Cannon, J. L., Mody, P. D., Blaine, K. M., Chen, E. J., Nelson, A. D., Sayles, L. J., Moore, T. V., Clay, B. S., Dulin, N. O., Shilling, R. A., Burkhardt, J. K., and Sperling, A. I. (2011) CD43 interaction with ezrin-radixin-moesin (ERM) proteins regulates T-cell trafficking and CD43 phosphorylation. *Mol. Biol. Cell* **22,** 954–963
55. Ilani, T., Khanna, C., Zhou, M., Veenstra, T. D., and Bretscher, A. (2007) Immune synapse formation requires ZAP-70 recruitment by ezrin and CD43 removal by moesin. *J. Cell Biol.* **179,** 733–746
56. Serrador, J. M., Nieto, M., Alonso-Lebrero, J. L., del Pozo, M. A., Calvo, J., Furthmayr, H., Schwartz-Albiez, R., Lozano, F., González-Amaro, R., Sánchez-Mateos, P., and Sánchez-Madrid, F. (1998) CD43 interacts with moesin and ezrin and regulates its redistribution to the uropods of T lymphocytes at the cell-cell contacts. *Blood* **91,** 4632–4644
57. Legg, J. W., and Isacke, C. M. (1998) Identification and functional analysis of the ezrin-binding site in the hyaluronan receptor, CD44. *Curr. Biol.* **8,** 705–708
58. Legg, J. W., Lewis, C. A., Parsons, M., Ng, T., and Isacke, C. M. (2002) A novel PKC-regulated mechanism controls CD44 ezrin association and directional cell motility. *Nat. Cell Biol.* **4,** 399–407
59. Li, Y., Harada, T., Juang, Y. T., Kyttaris, V. C., Wang, Y., Zidanic, M., Tung, K., and Tsokos, G. C. (2007) Phosphorylated ERM is responsible for increased T cell polarization, adhesion, and migration in patients with systemic lupus erythematosus. *J. Immunol.* **178,** 1938–1947
60. Mori, T., Kitano, K., Terawaki, S., Maesaki, R., Fukami, Y., and Hakoshima, T. (2008) Structural basis for CD44 recognition by ERM proteins. *J. Biol. Chem.* **283,** 29602–29612
61. Hao, J. J., Liu, Y., Kruhlak, M., Debell, K. E., Rellahan, B. L., and Shaw, S. (2009) Phospholipase C-mediated hydrolysis of PIP_2 releases ERM proteins from lymphocyte membrane. *J. Cell Biol.* **184,** 451–462
62. Tsukita, S., Oishi, K., Sato, N., Sagara, J., Kawai, A., and Tsukita, S. (1994) ERM family members as molecular linkers between the cell surface glycoprotein CD44 and actin-based cytoskeletons. *J. Cell Biol.* **126,** 391–401
63. Takahashi, K., Sasaki, T., Mammoto, A., Hotta, I., Takaishi, K., Imamura, H., Nakano, K., Kodama, A., and Takai, Y. (1998) Interaction of radixin with Rho small G protein GDP/GTP exchange protein Dbl. *Oncogene* **16,** 3279–3284
64. Tran Quang, C., Gautreau, A., Arpin, M., and Treisman, R. (2000) Ezrin function is required for ROCK-mediated fibroblast transformation by the Net and Dbl oncogenes. *EMBO J.* **19,** 4565–4576
65. Prag, S., Parsons, M., Keppler, M. D., Ameer-Beg, S. M., Barber, P., Hunt, J., Beavil, A. J., Calvert, R., Arpin, M., Vojnovic, B., and Ng, T. (2007) Activated ezrin promotes cell migration through recruitment of the GEF Dbl to lipid rafts and preferential downstream activation of Cdc42. *Mol. Biol. Cell* **18,** 2935–2948
66. Yang, H. S., and Hinds, P. W. (2006) Phosphorylation of ezrin by cyclin-dependent kinase 5 induces the release of Rho GDP dissociation inhibitor to inhibit Rac1 activity in senescent cells. *Cancer Res.* **66,** 2708–2715
67. Ognibene, M., Vanni, C., Segalerba, D., Mancini, P., Merello, E., Torrisi, M. R., Bosco, M. C., Varesio, L., and Eva, A. (2011) The tumor suppressor hamartin enhances Dbl protein transforming activity through interaction with ezrin. *J. Biol. Chem.* **286,** 29973–29983
68. Martín, M., Simon-Assmann, P., Kedinger, M., Martin, M., Mangeat, P., Real, F. X., and Fabre, M. (2006) DCC regulates cell adhesion in human colon cancer derived HT-29 cells and associates with ezrin. *Eur. J. Cell Biol.* **85,** 769–783
69. Antoine-Bertrand, J., Ghogha, A., Luangrath, V., Bedford, F. K., and Lamarche-Vane, N. (2011) The activation of ezrin-radixin-moesin proteins is regulated by netrin-1 through Src kinase and RhoA/Rho kinase activities and mediates netrin-1-induced axon outgrowth. *Mol. Biol. Cell* **22,** 3734–3746
70. Lue, R. A., Brandin, E., Chan, E. P., and Branton, D. (1996) Two independent domains of hDlg are sufficient for subcellular targeting: the PDZ1–2 conformational unit and an alternatively spliced domain. *J. Cell Biol.* **135,** 1125–1137
71. Lasserre, R., Charrin, S., Cuche, C., Danckaert, A., Thoulouze, M. I., de Chaumont, F., Duong, T., Perrault, N., Varin-Blank, N., Olivo-Marin, J. C., Etienne-Manneville, S., Arpin, M., Di Bartolo, V., and Alcover, A. (2010) Ezrin tunes T-cell activation by controlling Dlg1 and microtubule positioning at the immunological synapse. *EMBO J.* **29,** 2301–2314
72. LaLonde, D. P., and Bretscher, A. (2009) The scaffold protein PDZK1 undergoes a head-to-tail intramolecular association that negatively regulates its interaction with EBP50. *Biochemistry* **48,** 2261–2271
73. Zwaenepoel, I., Naba, A., Da Cunha, M. M., Del Maestro, L., Formstecher, E., Louvard, D., and Arpin, M. (2012) Ezrin regulates microvillus morphogenesis by promoting distinct activities of Eps8 proteins. *Mol. Biol. Cell* **23,** 1080–1094
74. Naba, A., Reverdy, C., Louvard, D., and Arpin, M. (2008) Spatial recruitment and activation of the Fes kinase by ezrin promotes HGF-induced cell scattering. *EMBO J.* **27,** 38–50
75. Helander, T. S., Carpén, O., Turunen, O., Kovanen, P. E., Vaheri, A., and Timonen, T. (1996) ICAM-2 redistributed by ezrin as a target for killer cells. *Nature* **382,** 265–268
76. Heiska, L., Alfthan, K., Grönholm, M., Vilja, P., Vaheri, A., and Carpén, O. (1998) Association of ezrin with intercellular adhesion molecule-1 and -2 (ICAM-1 and ICAM-2). Regulation by phosphatidylinositol 4, 5-bisphosphate. *J. Biol. Chem.* **273,** 21893–21900
77. Serrador, J. M., Alonso-Lebrero, J. L., del Pozo, M. A., Furthmayr, H., Schwartz-Albiez, R., Calvo, J., Lozano, F., and Sánchez-Madrid, F. (1997) Moesin interacts with the cytoplasmic region of intercellular adhesion molecule-3 and is redistributed to the uropod of T lymphocytes during cell polarization. *J. Cell Biol.* **138,** 1409–1423
78. Alonso-Lebrero, J. L., Serrador, J. M., Domínguez-Jiménez, C., Barreiro, O., Luque, A., del Pozo, M. A., Snapp, K., Kansas, G., Schwartz-Albiez, R., Furthmayr, H., Lozano, F., and Sánchez-Madrid, F. (2000) Polarization and interaction of adhesion molecules P-selectin glycoprotein ligand 1 and intercellular adhesion molecule 3 with moesin and ezrin in myeloid cells. *Blood* **95,** 2413–2419
79. Oh, H. M., Lee, S., Na, B. R., Wee, H., Kim, S. H., Choi, S. C., Lee, K. M., and Jun, C. D. (2007) RKIKK motif in the intracellular domain is critical for spatial and dynamic organization of ICAM-1: functional implication for the leukocyte adhesion and transmigration. *Mol. Biol. Cell* **18,** 2322–2335
80. Dickson, T. C., Mintz, C. D., Benson, D. L., and Salton, S. R. (2002) Functional binding interaction identified between the axonal CAM L1 and members of the ERM family. *J. Cell Biol.* **157,** 1105–1112
81. Sakurai, T., Gil, O. D., Whittard, J. D., Gazdoiu, M., Joseph, T., Wu, J., Waksman, A., Benson, D. L., Salton, S. R., and Felsenfeld, D. P. (2008) Interactions between the L1 cell adhesion molecule and ezrin support traction-force generation and can be regulated by tyrosine phosphorylation. *J. Neurosci. Res.* **86,** 2602–2614
82. Matsui, K., Parameswaran, N., Bagheri, N., Willard, B., and Gupta, N. (2011) Proteomics analysis of the ezrin interactome in B cells reveals a novel association with Myo18aα. *J. Proteome Res.* **10,** 3983–3992
83. Denker, S. P., Huang, D. C., Orlowski, J., Furthmayr, H., and Barber, D. L. (2000) Direct binding of the Na-H exchanger NHE1 to ERM proteins regulates the cortical cytoskeleton and cell shape independently of H^+ translocation. *Mol. Cell* **6,** 1425–1436
84. Denker, S. P., and Barber, D. L. (2002) Cell migration requires both ion translocation and cytoskeletal anchoring by the Na-H exchanger NHE1. *J. Cell Biol.* **159,** 1087–1096
85. Cha, B., Tse, M., Yun, C., Kovbasnjuk, O., Mohan, S., Hubbard, A., Arpin, M., and Donowitz, M. (2006) The NHE3 juxtamembrane cytoplasmic domain directly binds ezrin: dual role in NHE3 trafficking and mobility in the brush border. *Mol. Biol. Cell* **17,** 2661–2673
86. Mykkänen, O. M., Grönholm, M., Rönty, M., Lalowski, M., Salmikangas,

P., Suila, H., and Carpén, O. (2001) Characterization of human palladin, a microfilament-associated protein. *Mol. Biol. Cell* **12,** 3060–3073
87. Rachlin, A. S., and Otey, C. A. (2006) Identification of palladin isoforms and characterization of an isoform-specific interaction between Lasp-1 and palladin. *J. Cell Sci.* **119,** 995–1004
88. Henning, M. S., Stiedl, P., Barry, D. S., McMahon, R., Morham, S. G., Walsh, D., and Naghavi, M. H. (2011) PDZD8 is a novel moesin-interacting cytoskeletal regulatory protein that suppresses infection by herpes simplex virus type 1. *Virology* **415,** 114–121
89. D'Angelo, R., Aresta, S., Blangy, A., Del Maestro, L., Louvard, D., and Arpin, M. (2007) Interaction of ezrin with the novel guanine nucleotide exchange factor PLEKHG6 promotes RhoG-dependent apical cytoskeleton rearrangements in epithelial cells. *Mol. Biol. Cell* **18,** 4780–4793
90. Orlando, R. A., Takeda, T., Zak, B., Schmieder, S., Benoit, V. M., McQuistan, T., Furthmayr, H., and Farquhar, M. G. (2001) The glomerular epithelial cell anti-adhesin podocalyxin associates with the actin cytoskeleton through interactions with ezrin. *J. Am. Soc. Nephrol.* **12,** 1589–1598
91. Snapp, K. R., Heitzig, C. E., and Kansas, G. S. (2002) Attachment of the PSGL-1 cytoplasmic domain to the actin cytoskeleton is essential for leukocyte rolling on P-selectin. *Blood* **99,** 4494–4502
92. Serrador, J. M., Urzainqui, A., Alonso-Lebrero, J. L., Cabrero, J. R., Montoya, M. C., Vicente-Manzanares, M., Yáñez-Mó, M., and Sánchez-Madrid, F. (2002) A juxta-membrane amino acid sequence of P-selectin glycoprotein ligand-1 is involved in moesin binding and ezrin/radixin/moesin-directed targeting at the trailing edge of migrating lymphocytes. *Eur. J. Immunol.* **32,** 1560–1566
93. Takai, Y., Kitano, K., Terawaki, S., Maesaki, R., and Hakoshima, T. (2007) Structural basis of PSGL-1 binding to ERM proteins. *Genes Cells* **12,** 1329–1338
94. Domínguez-Luis, M., Lamana, A., Vazquez, J., García-Navas, R., Mollinedo, F., Sánchez-Madrid, F., Díaz-González, F., and Urzainqui, A. (2011) The metalloprotease ADAM8 is associated with and regulates the function of the adhesion receptor PSGL-1 through ERM proteins. *Eur. J. Immunol.* **41,** 3436–3442
95. Spertini, C., Baïsse, B., and Spertini, O. (2012) Ezrin-radixin-moesin-binding sequence of PSGL-1 glycoprotein regulates leukocyte rolling on selectins and activation of extracellular signal-regulated kinases. *J. Biol. Chem.* **287,** 10693–10702
96. Ramel, D., Wang, X., Laflamme, C., Montell, D. J., and Emery, G. (2013) Rab11 regulates cell-cell communication during collective cell movements. *Nat. Cell Biol.* **15,** 317–324
97. Sperka, T., Geissler, K. J., Merkel, U., Scholl, I., Rubio, I., Herrlich, P., and Morrison, H. L. (2011) Activation of Ras requires the ERM-dependent link of actin to the plasma membrane. *PLoS One* **6,** e27511
98. Takahashi, K., Sasaki, T., Mammoto, A., Takaishi, K., Kameyama, T., Tsukita, S., and Takai, Y. (1997) Direct interaction of the Rho GDP dissociation inhibitor with ezrin/radixin/moesin initiates the activation of the Rho small G protein. *J. Biol. Chem.* **272,** 23371–23375
99. Koltzscher, M., Neumann, C., König, S., and Gerke, V. (2003) Ca^{2+}-dependent binding and activation of dormant ezrin by dimeric S100P. *Mol. Biol. Cell* **14,** 2372–2384
100. Austermann, J., Nazmi, A. R., Müller-Tidow, C., and Gerke, V. (2008) Characterization of the Ca^{2+}-regulated ezrin-S100P interaction and its role in tumor cell migration. *J. Biol. Chem.* **283,** 29331–29340
101. Bonilha, V. L., and Rodriguez-Boulan, E. (2001) Polarity and developmental regulation of two PDZ proteins in the retinal pigment epithelium. *Invest. Ophthalmol. Vis. Sci.* **42,** 3274–3282
102. Chirivino, D., Del Maestro, L., Formstecher, E., Hupé, P., Raposo, G., Louvard, D., and Arpin, M. (2011) The ERM proteins interact with the HOPS complex to regulate the maturation of endosomes. *Mol. Biol. Cell* **22,** 375–385
103. Jin, C., Ge, L., Ding, X., Chen, Y., Zhu, H., Ward, T., Wu, F., Cao, X., Wang, Q., and Yao, X. (2006) PKA-mediated protein phosphorylation regulates ezrin-WWOX interaction. *Biochem. Biophys. Res. Commun.* **341,** 784–791
104. Zaarour, R. F., Chirivino, D., Del Maestro, L., Daviet, L., Atfi, A., Louvard, D., and Arpin, M. (2012) Ezrin ubiquitylation by the E3 ubiquitin ligase, WWP1, and consequent regulation of hepatocyte growth factor receptor activity. *PLoS One* **7,** e37490
105. Wan, X., Kim, S. Y., Guenther, L. M., Mendoza, A., Briggs, J., Yeung, C., Currier, D., Zhang, H., Mackall, C., Li, W. J., Tuan, R. S., Deyrup, A. T., Khanna, C., and Helman, L. (2009) β4 integrin promotes osteosarcoma metastasis and interacts with ezrin. *Oncogene* **28,** 3401–3411